JLAB-XX-XXX
MSUHEP-XX-XXX

Extraction of the x-dependence of generalized parton distributions from exclusive photoproduction

Jian-Wei Qiu[1, 2, *] and Zhite Yu[3, †]

[1] *Theory Center, Jefferson Lab, Newport News, Virginia 23606, USA*
[2] *Department of Physics, William & Mary, Williamsburg, Virginia 23187, USA*
[3] *Department of Physics and Astronomy, Michigan State University, East Lansing, MI 48824, USA*

(Dated: May 23, 2023)

The x-dependence of hadrons' generalized parton distributions (GPDs) $\mathcal{F}(x,\xi,t)$ is the most difficult to extract from the existing known processes, while the ξ and t dependence are uniquely determined by the kinematics of the scattered hadron. We study the single diffractive hard exclusive processes for extracting GPDs in the photoproduction. We demonstrate quantitatively the enhanced sensitivity on extracting the x-dependence of various GPDs from the photoproduction cross sections, as well as the asymmetries constructed from photon polarization and hadron spin that could be measured at JLab Hall D by GlueX Collaboration and future facilities.

Introduction.—The generalized parton distributions (GPDs), $\mathcal{F}(x,\xi,t)$, provide rich information on the confined spatial distributions of quarks and gluons inside a bound hadron (for reviews, see [1–4]). The Fourier transform of their t-dependence at the forward limit $\xi \to 0$ provides tomographic quark/gluon images of the hadron in its transverse plane as functions of the active parton momentum fraction x [5, 6]. The x-moments of GPDs are responsible for many emergent hadronic properties such as the hadron's mass [7–10] and spin [11], as well as its internal pressure and shear force [12, 13].

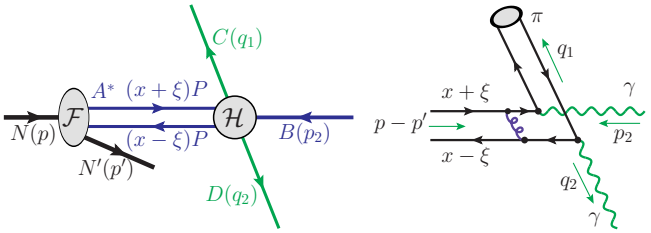

Fig. 1. (a) Sketch of $2 \to 3$ SDHEP needed for extracting GPDs. (b) Sample diagram for the SDHEP in Eq. (1).

Experimental measurement of GPDs requires a $2 \to 3$ exclusive process at a minimum, as sketched in Fig. 1(a), in which a hadron N of momentum p is scattered (or diffracted) to a hadron N' of momentum p' by exchanging a virtual two-parton state A^* of momentum $\Delta \equiv p - p'$ and invariant mass $t = \Delta^2$, which undergoes a hard exclusive scattering with the colliding particle $B =$ (lepton, photon, pion) of momentum p_2 to produce two back-to-back particles $C(q_1)$ and $D(q_2)$. To ensure the separation between the hard scattering $\mathcal{H}$ and the probed GPD $\mathcal{F}$, it is necessary to require the transverse momentum of the produced particles C and D to be much larger than the invariant mass of the exchange state A^*, $|q_{1T}| = |q_{2T}| \equiv q_T \gg \sqrt{|t|}$ (or equivalently, the hard collision time to be much shorter than the lifetime of the A^*) to suppress the quantum interference between the $\mathcal{H}$ and $\mathcal{F}$ [14, 15]. We referred to such an exclusive process for extracting GPDs as single diffractive hard exclusive process (SDHEP). A number of $2 \to 3$ SDHEPs have been proposed for extracting GPDs [16–25], among which is the deeply virtual Compton scattering (DVCS) [16, 17], corresponding to $B = C =$ electron and $D = \gamma$. In addition, a few $2 \to 4$ SDHEPs have also been proposed for extracting GPDs [26–29]. However, most of the processes proposed, including DVCS, do not give strong constraints on the x-dependence of GPDs [30].

Once the scattered hadron momentum p' is measured, the t, $\xi \equiv [\Delta \cdot n / 2P \cdot n]$ with $P = (p + p')/2$ and $n = (0^+, 1^-, \mathbf{0}_T)$ defining the leading momentum component, and the collision energy of the hard exclusive subprocess $(p - p' + p_2)^2$ are fully determined. For an SDHEP to be sensitive to the x-dependence of GPDs, the remaining freedom of the hard subprocess H, such as the q_T (or the angle) of the produced particle C or D, needs to be *entangled* with x, which is proportional to the relative momentum of the two exchanged partons [15]. For the DVCS, the exchange state $A^*(p - p')$ in Fig. 1 can be a virtual photon for the Bethe-Heitler process, a $q\bar{q}$ pair for quark GPDs and a pair of gluons for gluon GPDs if we neglect terms further suppressed by powers of $Q^2 = -(p_2 - q_1)^2$. Since the relative momentum of the two exchanged partons is decoupled from external variation of Q^2 at leading order, the measured DVCS cross sections probe GPDs through their "moment", like $\int dx\, \mathcal{F}(x,\xi,t)/(x-\xi)$ [15], which makes very difficult to extract the full x-dependence of GPDs [30]. Although QCD evolution of GPDs could introduce some sensitivity to the x-dependence [31], the event rate drops very quickly when Q^2 increases.

In this Letter, we study the sensitivity in extracting

GPDs from exclusive photoproduction [15, 32, 33],

$$N(p) + \gamma(p_2) \to N'(p') + \pi(q_1) + \gamma(q_2). \qquad (1)$$

The corresponding QCD factorization was justified in Ref. [15] by treating this process as a crossing process of the exclusive diphoton production in diffractive pion-nucleon collisions [14]. We calculate the leading-order (LO) short-distance hard parts and find that the transverse momentum (or the polar angle θ) of the final-state pion (or photon) is clearly entangled with the relative momentum of the two exchanged partons. Variation of observed q_T can provide enhanced sensitivity to the x-dependence of GPDs. With the crossing kinematics, this process provides more enhanced x-sensitivity in the ERBL region of GPDs (with $|x| \le |\xi|$), while the diphoton production in pion-nucleon scattering is more sensitive to the GPDs' DGLAP region ($|x| > |\xi|$) [14]. In addition, with the well-controlled polarization of the initial-state photon beam at JLab Hall D [34] and polarized hadron targets, we introduce asymmetries of cross sections constructed from the photon beam polarization and target spin and demonstrate quantitatively the enhanced capability of extracting various GPDs and their x-dependence from measurements at JLab Hall D and future facilities.

Kinematics and observables.—In Fig. 2, we describe the kinematics of the SDHEP in Eq. (1) in terms of two frames and two planes. The *Lab frame* is chosen to be the center-of-mass (c.m.) frame of the colliding hadron $N(p)$ and photon $\gamma(p_2)$ with the $\hat{z}_{\rm lab}$ along the momentum p, and $\hat{x}_{\rm lab}$ in the $N \to N'$ *diffractive plane* defined by the momentum p and p'. The *SDHEP frame* is the c.m. frame of the final-state π-γ pair, which is the same as the c.m. of the hard scattering subprocess, with $\hat{z}$ along the momentum Δ of A^*, while the initial-state photon along the $-\hat{z}$ direction and $\hat{x}$ lying on the diffractive plane as shown in Fig. 2. The $\hat{z}$ and the observed π momentum q_1 define the *scattering plane*, and the angles (θ, ϕ) define the direction of the observed π in the SDHEP frame. Choosing the $(\hat{x}_{\rm lab}, \hat{z}_{\rm lab})$ and $(\hat{x}, \hat{z})$ of these two frames on the same diffractive plane makes the Lorentz transformation between them simpler.

The SDHEP frame in Fig. 2 is very similar to the Breit frame for describing the lepton-hadron semi-inclusive deep inelastic scattering (SIDIS) in the Trento convention [35] if one corresponds the hadron N and N' to the colliding electron and scattered electron in SIDIS, respectively, and the diffractive plane and scattering plane to the leptonic plane and hadronic plane in SIDIS, respectively. But, unlike the virtual photon exchanged between the colliding lepton and hadron in SIDIS, the $A^*(\Delta)$ is a "long-lived" state with a low enough virtuality.

Both the colliding photon and hadron target at JLab Hall D can be polarized longitudinally. In addition, the photon can have linear polarization ζ and the hadron

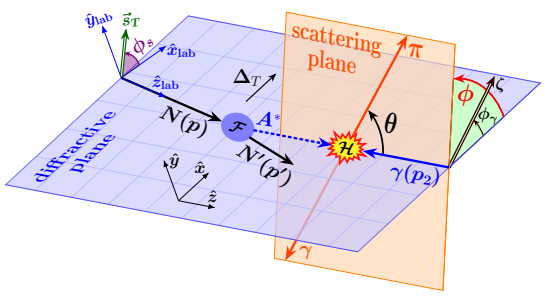

Fig. 2. Frames for the process in Eq. (1). The vectors of $\boldsymbol{s}_T$ and ζ refer to the transverse spin and linear polarization of the colliding nucleon N and photon γ, respectively.

can have a transverse spin s_T, defined by the azimuthal angles, ϕ_γ and ϕ_s in the Lab frame, respectively.

Having a pion in the final state eliminates the contribution from A^* being a virtual photon due to charge parity, so that the leading contribution to the SDHEP in Eq. (1) is from channels with A^* being a collinear parton pair. The corresponding scattering amplitude can be factorized into GPDs for the hadron transition $N \to N'$, a distribution amplitude (DA) for the formation of the final-state pion, and perturbatively calculable coefficients [15]

$$\mathcal{M}^{[\mathcal{F},\widetilde{F}]}_{N\gamma_\lambda \to N'\pi\gamma_{\lambda'}} = \sum_{f,f'} \int_{-1}^{1} dx \int_0^1 dz\, \bar{D}_{f'/\pi}(z) \qquad (2)$$
$$\times \left[\mathcal{F}^f_{NN'}(x,\xi,t)\, \widetilde{C}^{ff'}_{\lambda\lambda'}(x,z) + \widetilde{\mathcal{F}}^f_{NN'}(x,\xi,t)\, C^{ff'}_{\lambda\lambda'}(x,z) \right],$$

where $f = [q\bar{q}]$ and $[gg]$ for quark and gluon GPDs, respectively, if $N' = N$, or $f = [q\bar{q}']$ for transition GPDs with $N \neq N'$, and correspondingly, $f' = [q\bar{q}]$ or $[q\bar{q}']$ with $\bar{D}_{f'/\pi}$ being the DA for the produced pion. The hard coefficients $C^{ff'}_{\lambda\lambda'}$ and $\widetilde{C}^{ff'}_{\lambda\lambda'}$ are helicity amplitudes for the photon scattering off a collinear on-shell parton pair f with λ and λ' denoting the photon helicities in the SDHEP frame. Under the parity invariance, they can be reduced to four independent amplitudes, two helicity-conserving ones (C_+, $\widetilde{C}_+$) and two helicity-flipping ones (C_-, $\widetilde{C}_-$). Their explicit forms are collected in the Supplemental Material. The correction to the factorization in Eq. (2) is suppressed by powers of $|t|/q_T^2 \ll 1$.

The differential cross section for the SDHEP in Eq. (1) is

$$\frac{d\sigma}{d|t|\, d\xi\, d\cos\theta\, d\phi} = \frac{1}{2\pi} \frac{d\sigma}{d|t|\, d\xi\, d\cos\theta} \cdot \big[1 + \lambda_N \lambda_\gamma\, A_{LL}$$
$$+ \zeta\, A_{UT} \cos 2(\phi - \phi_\gamma) + \lambda_N\, \zeta A_{LT} \sin 2(\phi - \phi_\gamma)\big], \quad (3)$$

where λ_N and λ_γ are the net helicities of the initial-state nucleon and photon, respectively. In Eq. (3), we introduced the unpolarized differential cross section,

$$\frac{d\sigma}{d|t|\, d\xi\, d\cos\theta} = \frac{\mathcal{N}^2\,(1-\xi)}{32\, s\, (2\pi)^3\, (1+\xi)} \Sigma_{UU}, \qquad (4)$$

where $\mathcal{N}$ is a normalization factor defined below Eq. (S1), and polarization asymmetries,

$$\begin{aligned}
\Sigma_{UU} &= |\mathcal{M}_+^{[\widetilde{H}]}|^2 + |\mathcal{M}_-^{[\widetilde{H}]}|^2 + |\widetilde{\mathcal{M}}_+^{[H]}|^2 + |\widetilde{\mathcal{M}}_-^{[H]}|^2, \\
A_{LL} &= 2\,\Sigma_{UU}^{-1}\,\mathrm{Re}\left[\mathcal{M}_+^{[\widetilde{H}]}\,\widetilde{\mathcal{M}}_+^{[H]*} + \mathcal{M}_-^{[\widetilde{H}]}\,\widetilde{\mathcal{M}}_-^{[H]*}\right], \\
A_{UT} &= 2\,\Sigma_{UU}^{-1}\,\mathrm{Re}\left[\widetilde{\mathcal{M}}_+^{[H]}\,\widetilde{\mathcal{M}}_-^{[H]*} - \mathcal{M}_+^{[\widetilde{H}]}\,\mathcal{M}_-^{[\widetilde{H}]*}\right], \\
A_{LT} &= 2\,\Sigma_{UU}^{-1}\,\mathrm{Im}\left[\mathcal{M}_+^{[\widetilde{H}]}\,\widetilde{\mathcal{M}}_-^{[H]*} + \mathcal{M}_-^{[\widetilde{H}]}\,\widetilde{\mathcal{M}}_+^{[H]*}\right], \qquad (5)
\end{aligned}$$

whose two subscripts are for hadron spin and photon polarization, respectively, with U for "unpolarized", L for "longitudinal polarized", and T for "linearly polarized photon", leaving the situation of transversely polarized hadron to a future publication. The helicity amplitudes $\mathcal{M}_\pm^{[\widetilde{H}]}$ and $\widetilde{\mathcal{M}}_\pm^{[H]}$ in Eq. (5) are given in Eqs. (S8)-(S11) in terms of convolutions of GPD $\widetilde{H}$ and H, respectively, with corresponding hard coefficients. In this Letter, we focus on contributions from quark GPDs and leave the contribution of gluon GPDs to a future publication.

Enhanced x-sensitivity.—While GPDs' t and ξ dependence can be directly measured, their x dependence (as well as the z dependence of DA) is only probed via convolutions as in Eq. (2). As explained in Ref. [15], the LO hard coefficient C for almost all known processes for extracting GPDs has its x dependence decoupled from the measured hard scale(s), e.g., for DVCS [16, 17],

$$C_{\mathrm{DVCS}}^{\mathrm{LO}}(x,\xi;x_B,Q^2) = \frac{1}{x\pm\xi\mp i\varepsilon}\,C(x_B,Q^2)\,. \qquad (6)$$

Consequently, experimental variation of the probing scale of these processes has little influence on the x convolution of GPDs. Since the unpinched x poles in Eq. (6) are only localized at $\pm\xi$, experimental measurements of DVCS may only constrain the diagonal values of GPDs $\mathcal{F}(\xi,\xi,t)$ through the imaginary parts and the limited "moments",

$$\mathcal{F}_0(\xi,t) = \mathcal{P}\int_{-1}^{1} dx \frac{\mathcal{F}(x,\xi,t)}{x-\xi}, \qquad (7)$$

with $\mathcal{P}$ indicating principle-value integration. Such lack of sensitivity to the full x dependence of GPDs is also true for other known processes, including the deeply virtual meson production (DVMP) [18, 19], photoproduction of lepton [20] or photon pair [24, 36, 37], and the exclusive Drell-Yan process [21].

Having only the moment sensitivity is far from enough to map out the x distribution of GPDs. One can easily construct null solutions to Eq. (7) that give zero to the moments, diagonal values and forward limits [30]. Such solutions are termed shadow GPDs, which are invisible to processes that only possess moment-type sensitivity. Although QCD evolution of GPDs in response to the variation of the probing scale might help with this situation [38], the nature of logarithmic high-order contributions makes the improvement numerically not appreciable [30] unless one goes to a sufficiently high scale [31] where the cross section itself diminishes, which makes it difficult to reach the desired precision.

However, the hard coefficients for the SDHEP in Eq. (1), as shown in Eqs. (S2)-(S5), have not only terms in which the x dependence is decoupled from the external hard scale q_T (or equivalently, the polar angle θ) of the observed pion in the SDHEP frame, like that in Eq. (6), but also terms in which the x dependence cannot be factorized as in Eq. (6) and is entangled with the observed q_T (or θ). More precisely, the helicity-conserving hard coefficients C_+ in Eq. (S2) and $\widetilde{C}_+$ in Eq. (S4) contain terms proportional to e_1e_2, in which the external observable θ is entangled with the partons' momentum fractions x and z. Their convolutions with GPD H and $\widetilde{H}$ lead to the following type of integrals,

$$\int_{-1}^{1} dx \frac{(H^+,\widetilde{H}^+)(x,\xi,t)}{x-x_p(\xi,z,\theta)+i\epsilon}\,, \qquad (8)$$

with the x pole away from $\pm\xi$ and entangled with the externally measured θ in the form,

$$x_p(\xi,z,\theta) = \xi\cdot\left[\frac{\cos^2(\theta/2)(1-z)-z}{\cos^2(\theta/2)(1-z)+z}\right]. \qquad (9)$$

Such contribution arises from Feynman diagrams with the two photons attached to two different fermion lines, like the one in Fig. 1(b), so that the momentum flow through the short-distance gluon contains both x dependence from the GPD (and z dependence from DA) and q_T (or θ) dependence. This special gluon propagator is responsible for the x_p form in Eq. (9). Such entanglement provides *enhanced sensitivity* to the x dependence of GPDs from the experimentally measured q_T or θ distribution. With z going from 0 to 1, x_p in Eq. (9) goes from ξ to $-\xi$, scanning through the whole ERBL region of GPDs. This is complementary to the high-q_T diphoton production in single diffractive pion-nucleon scattering, which is capable of scanning through the whole DGLAP region of GPDs [14].

The four helicity amplitudes $\mathcal{M}_\pm^{[\widetilde{H}]}$ and $\widetilde{\mathcal{M}}_\pm^{[H]}$ cannot be distinguished by considering only the unpolarized differential cross section in Eq. (4), from which the two amplitudes $\mathcal{M}_+^{[\widetilde{H}]}$ and $\widetilde{\mathcal{M}}_+^{[H]}$ with enhanced x-sensitivity cannot be distinguished. Fortunately, with the capability of polarizing both the photon beam and hadron target at JLab, various polarization asymmetries can be constructed as shown in Eq. (5). The single spin asymmetry, A_{UT}, mixes the helicity-conserving and flipping amplitudes, and then depends more on the amplitudes with enhanced x-sensitivity, especially on their absolute signs. The double spin asymmetries, A_{LL} and A_{LT}, provide different combinations of the GPD H and $\widetilde{H}$. In particular,

A_{LT} is given by the imaginary parts of the amplitudes, which probe the GPD values in the ERBL region due to the special x pole at $x_p(\xi, z, \theta)$ in Eq. (9).

The unpolarized cross section plus three asymmetries in Eq. (5) can provide good information to disentangle the four GPDs $H_\pm$ and $\widetilde{H}_\pm$. If the hadron can also be transversely polarized, the associated asymmetry can provide new information to add constraints on the GPD E and $\widetilde{E}$, which is beyond the scope of this Letter.

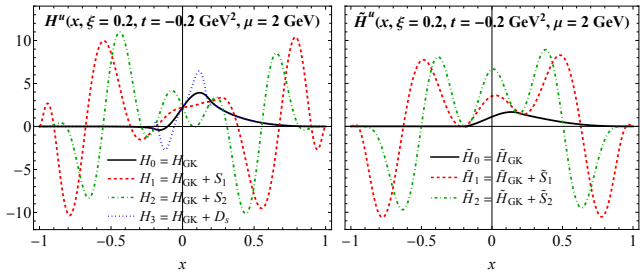

Fig. 3. Choices of the u-quark GPD models at $t = -0.2$ GeV^2 and $\xi = 0.2$, by adding shadow GPDs to the GK model.

Numerical results.—The CEBAF at JLab is capable of delivering intense polarized photon beam to its Hall D to study the SDHEP in Eq. (1) on various hadron targets, which can also be polarized. We evaluate the production rate and various asymmetries in Eq. (5) to demonstrate the enhanced x-sensitivity on extracting GPDs. We take the GK model [39–42] as the reference GPD for H and $\widetilde{H}$, referred as H_0 and $\widetilde{H}_0$, respectively. As shown in Fig. 3, we construct additional GPDs H_i and $\widetilde{H}_i$ with different x-dependence from modifying the reference u-quark GPD by adding various shadow GPDs, $S_i(x, \xi)$ or $\widetilde{S}_i(x, \xi)$, or a shadow D-term $D_s(x/\xi)$, which are constructed (in the Supplemental Material) to give zero contribution to the GPD's forward limit and its moment in Eq. (7). We fix the pion DA to be its asymptotic form [43]. In order to focus on the x-sensitivity from the q_T (or θ) distribution of this particular process, we neglect evolution effects of GPDs and fix both renormalization and factorization scales at 2 GeV.

In Fig. 4, we show the unpolarized differential cross section in Eq. (4) together with the various asymmetries in Eq. (5) for π^0 production as a function of its polar angle θ in the SDHEP frame at $E_\gamma = 9$ GeV. Since the $\cos\theta$-dependence is multiplicative to the x/z-dependence of hard coefficients C_- and $\widetilde{C}_-$, the shadow GPDs are not visible to them. On the other hand, the $\cos\theta$-dependence of C_+ and $\widetilde{C}_+$ is entangled with their x/z-dependence, and therefore, GPDs with different x-dependence lead to the different rate and asymmetries. In particular, the A_{LT} is sensitive to the imaginary parts of the amplitudes, which are generated in the ERBL region, and has a better sensitivity to the shadow D-term than the other three observables as shown in Fig. 4. In general, the oscillation of shadow GPDs in the DGLAP region causes a

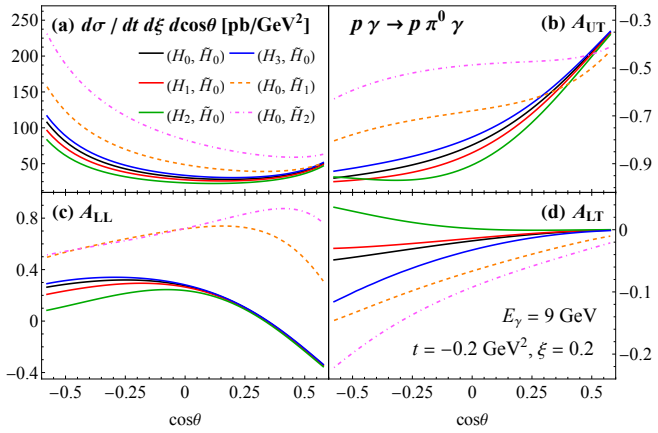

Fig. 4. Unpolarized rate (a) and polarization asymmetries (b)-(d) as functions of $\cos\theta$ at $(t, \xi) = (-0.2\ \text{GeV}^2, 0.2)$, using different GPD sets as given in Fig. 3.

big cancellation in their contribution to the amplitudes, while the sensitivity is more positively correlated with the GPD magnitude in the ERBL region. The shadow $\widetilde{S}_i$, associated with the x-dependence of the polarized GPD $\widetilde{H}$ gives bigger contribution to the amplitude $\mathcal{M}_+^{[\widetilde{S}]}$ than S_i to $\widetilde{\mathcal{M}}_+^{[S]}$ due to charge symmetry property, so that they can be better probed.

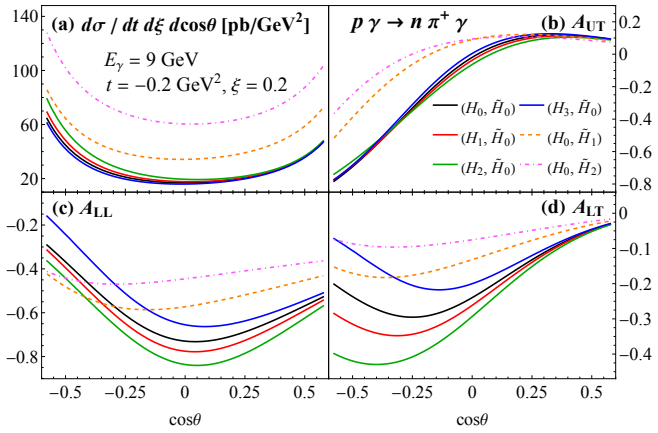

Fig. 5. Same as Fig. 4, but for the $p\gamma \to n\pi^+\gamma$ process.

For the neutral pion production, we can eliminate terms proportional to $(e_1 - e_2)^2$ or $(e_1^2 - e_2^2)$ in the hard coefficients in Eqs. (S2)-(S5) since $e_1 = e_2$, which effectively removes a good number of moment-type terms, giving the maximum amount of entanglement and the most sensitivity to GPDs' x-dependence. In Fig. 5, we present the same study for the $p\gamma \to n\pi^+\gamma$ process. With different flavor combination, it provides different x-sensitivity. The $n\gamma \to p\pi^-\gamma$ process gives a similar result, but with a smaller production rate. As demonstrated in Figs. 4 and 5, both the production rate and asymmetries are sizable

and measurable, making the SDHEP in Eq. (1) uniquely different from DVCS and others in terms of its enhanced sensitivity for extracting the x-dependence of GPDs.

Summary and outlook.—Extracting the full x dependence of GPDs is very important not only for probing the tomographic partonic images of hadrons, but also for predicting and understanding the emergent hadron properties in terms of various moments of GPDs. However, the fact that the most known processes for extracting GPDs, including DVCS and DVMP, have only moment-type sensitivity makes it very difficult, if not impossible, to pin down the x-dependence of GPDs and their flavor dependence due to the possibility of having an infinite number of shadow GPDs which are hardly visible to these processes.

In this Letter, we demonstrated quantitatively that the SDHEP in Eq. (1) is not only accessible by JLab Hall D but also capable of providing much enhanced sensitivity to the x-dependence of GPDs, as well as the potential to probe the flavor dependence of GPDs from the production rates and various asymmetries. This is possible because this process has the entanglement of the x flow of GPDs with the externally observed hard scale [14, 15], which is a critical criterion for searching for good physical processes to help extract the x dependence of GPDs. Since multiple GPDs could contribute to the same observables through convolutions of their x-dependence, extracting GPDs from data is a challenging inverse problem. A global analysis of multiple processes is necessary for extracting these nonperturbative and universal GPDs from which we can picture the spatial distribution of the probability densities to find quarks and gluons inside a bound hadron. With the full knowledge of the x dependence of GPDs, we would be able to not only address how partonic dynamics impacts the emergent hadronic properties, but also provide quantitative answers to profound questions, including what the proton radius is in terms of its transverse spatial distribution of quarks, $r_q(x)$, or gluons, $r_g(x)$, how such radii compare with its electromagnetic charge radius, and how far from the center of the proton the quarks and gluons could still be found.

Acknowledgments.—We thank N. Sato, J. Stevens and M. Strikman for helpful discussions and communications. This work is supported in part by the US Department of Energy (DOE) Contract No. DE-AC05-06OR23177, under which Jefferson Science Associates, LLC operates Jefferson Lab. The work of Z.Y. at MSU is partially supported by the U.S. National Science Foundation under Grant No. PHY-2013791, and the fund from the Wu-Ki Tung endowed chair in particle physics.

* jqiu@jlab.org
† yuzhite@msu.edu

[1] K. Goeke, M. V. Polyakov, and M. Vanderhaeghen, Prog. Part. Nucl. Phys. **47**, 401 (2001), hep-ph/0106012.
[2] M. Diehl, Phys. Rept. **388**, 41 (2003), hep-ph/0307382.
[3] A. V. Belitsky and A. V. Radyushkin, Phys. Rept. **418**, 1 (2005), hep-ph/0504030.
[4] S. Boffi and B. Pasquini, Riv. Nuovo Cim. **30**, 387 (2007), 0711.2625.
[5] M. Burkardt, Phys. Rev. D **62**, 071503 (2000), [Erratum: Phys.Rev.D 66, 119903 (2002)], hep-ph/0005108.
[6] M. Burkardt, Int. J. Mod. Phys. A **18**, 173 (2003), hep-ph/0207047.
[7] X.-D. Ji, Phys. Rev. Lett. **74**, 1071 (1995), hep-ph/9410274.
[8] X.-D. Ji, Phys. Rev. D **52**, 271 (1995), hep-ph/9502213.
[9] C. Lorcé, Eur. Phys. J. C **78**, 120 (2018), 1706.05853.
[10] A. Metz, B. Pasquini, and S. Rodini, Phys. Rev. D **102**, 114042 (2020), 2006.11171.
[11] X.-D. Ji, Phys. Rev. Lett. **78**, 610 (1997), hep-ph/9603249.
[12] M. V. Polyakov and P. Schweitzer, Int. J. Mod. Phys. A **33**, 1830025 (2018), 1805.06596.
[13] V. D. Burkert, L. Elouadrhiri, and F. X. Girod, Nature **557**, 396 (2018).
[14] J.-W. Qiu and Z. Yu, JHEP **08**, 103 (2022), 2205.07846.
[15] J.-W. Qiu and Z. Yu, Phys. Rev. D **107**, 014007 (2023), 2210.07995.
[16] X.-D. Ji, Phys. Rev. D **55**, 7114 (1997), hep-ph/9609381.
[17] A. V. Radyushkin, Phys. Rev. D **56**, 5524 (1997), hep-ph/9704207.
[18] S. J. Brodsky, L. Frankfurt, J. F. Gunion, A. H. Mueller, and M. Strikman, Phys. Rev. D **50**, 3134 (1994), hep-ph/9402283.
[19] L. Frankfurt, W. Koepf, and M. Strikman, Phys. Rev. D **54**, 3194 (1996), hep-ph/9509311.
[20] E. R. Berger, M. Diehl, and B. Pire, Eur. Phys. J. C **23**, 675 (2002), hep-ph/0110062.
[21] E. R. Berger, M. Diehl, and B. Pire, Phys. Lett. B **523**, 265 (2001), hep-ph/0110080.
[22] S. Kumano, M. Strikman, and K. Sudoh, Phys. Rev. D **80**, 074003 (2009), 0905.1453.
[23] M. El Beiyad, B. Pire, M. Segond, L. Szymanowski, and S. Wallon, Phys. Lett. B **688**, 154 (2010), 1001.4491.
[24] A. Pedrak, B. Pire, L. Szymanowski, and J. Wagner, Phys. Rev. D **96**, 074008 (2017), [Erratum: Phys.Rev.D 100, 039901 (2019)], 1708.01043.
[25] M. Siddikov and I. Schmidt, Phys. Rev. D **107**, 034037 (2023), 2212.14019.
[26] M. Guidal and M. Vanderhaeghen, Phys. Rev. Lett. **90**, 012001 (2003), hep-ph/0208275.
[27] A. V. Belitsky and D. Mueller, Phys. Rev. Lett. **90**, 022001 (2003), hep-ph/0210313.
[28] A. V. Belitsky and D. Mueller, Phys. Rev. D **68**, 116005 (2003), hep-ph/0307369.
[29] A. Pedrak, B. Pire, L. Szymanowski, and J. Wagner, Phys. Rev. D **101**, 114027 (2020), 2003.03263.
[30] V. Bertone, H. Dutrieux, C. Mezrag, H. Moutarde, and P. Sznajder, Phys. Rev. D **103**, 114019 (2021), 2104.03836.
[31] E. Moffat, A. Freese, I. Cloët, T. Donohoe, L. Gamberg, W. Melnitchouk, A. Metz, A. Prokudin, and N. Sato (2023), 2303.12006.
[32] G. Duplančić, K. Passek-Kumerički, B. Pire, L. Szymanowski, and S. Wallon, JHEP **11**, 179 (2018), 1809.08104.

[33] G. Duplančić, S. Nabeebaccus, K. Passek-Kumerički, B. Pire, L. Szymanowski, and S. Wallon, JHEP **03**, 241 (2023), 2212.00655.
[34] H. Al Ghoul et al. (GlueX), Phys. Rev. C **95**, 042201 (2017), 1701.08123.
[35] A. Bacchetta, U. D'Alesio, M. Diehl, and C. A. Miller, Phys. Rev. D **70**, 117504 (2004), hep-ph/0410050.
[36] O. Grocholski, B. Pire, P. Sznajder, L. Szymanowski, and J. Wagner, Phys. Rev. D **104**, 114006 (2021), 2110.00048.
[37] O. Grocholski, B. Pire, P. Sznajder, L. Szymanowski, and J. Wagner, Phys. Rev. D **105**, 094025 (2022), 2204.00396.
[38] A. Freund, Phys. Lett. B **472**, 412 (2000), hep-ph/9903488.
[39] S. V. Goloskokov and P. Kroll, Eur. Phys. J. C **42**, 281 (2005), hep-ph/0501242.
[40] S. V. Goloskokov and P. Kroll, Eur. Phys. J. C **53**, 367 (2008), 0708.3569.
[41] S. V. Goloskokov and P. Kroll, Eur. Phys. J. C **65**, 137 (2010), 0906.0460.
[42] P. Kroll, H. Moutarde, and F. Sabatie, Eur. Phys. J. C **73**, 2278 (2013), 1210.6975.
[43] G. P. Lepage and S. J. Brodsky, Phys. Rev. D **22**, 2157 (1980).
[44] F. X. Girod et al. (CLAS), Phys. Rev. Lett. **100**, 162002 (2008), 0711.4805.
[45] H. S. Jo et al. (CLAS), Phys. Rev. Lett. **115**, 212003 (2015), 1504.02009.

SUPPLEMENTAL MATERIAL

Hard coefficients for the photon-proton scattering process

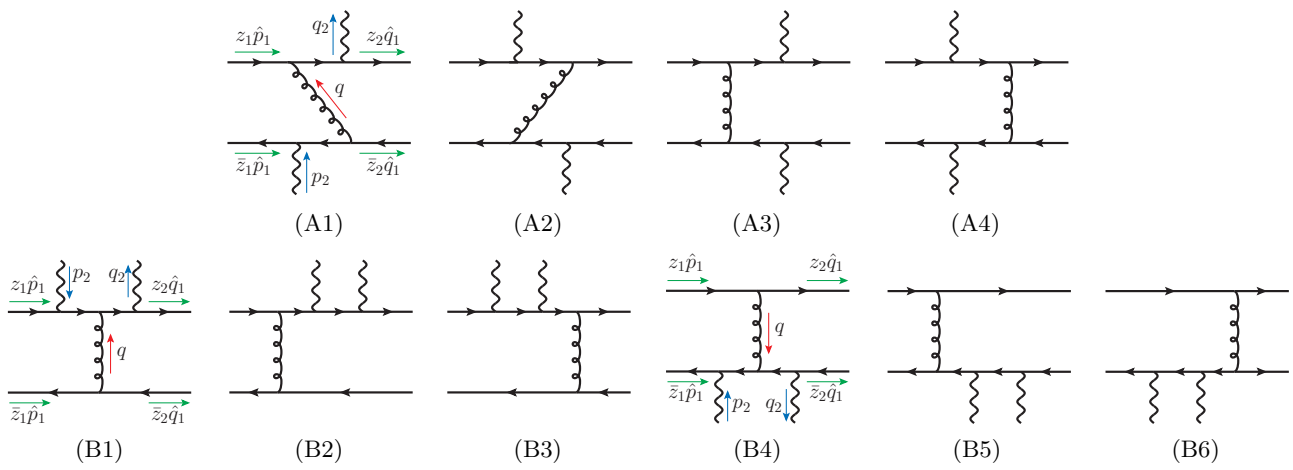

Fig. S1. Hard scattering diagrams for the photon-proton scattering into a photon-pion pair. They can be calculated by following the two-stage paradigm described in Fig. 1(a). The two incoming fermion lines on the left are from the diffracted nucleon, carrying momenta $z_1\hat{p}_1$ and $\bar{z}_1\hat{p}_1 \equiv (1-z_1)\hat{p}_1$, respectively, where $\hat{p}_1 = (\Delta\cdot n)\bar{n}$ with $n = (0^+, 1^-, \mathbf{0}_T)$ and $\bar{n} = (1^-, 0^+, \mathbf{0}_T)$. The two outgoing fermion lines on the right are to form the produced pion, carrying momenta $z_2\hat{q}_1$ and $\bar{z}_2\hat{q}_1 \equiv (1-z_2)\hat{q}_1$, respectively, where $\hat{q}_1 = (q_1\cdot w)\bar{w}$ with w and $\bar{w}$ like n and $\bar{n}$, respectively, but with $\hat{z}$-axis along $\vec{q}_1$. The variables z_1 and z_2 are related to x and z by $z_1 = (x+\xi)/2\xi$ and $z_2 = z$ (see the text). Another set of diagrams are also to be included by switching the two photon lines, giving 20 diagrams in total.

The hard coefficients $\widetilde{C}_{\lambda\lambda'}$ ($C_{\lambda\lambda'}$) for the photon-proton scattering process are obtained from the diagrams in Fig. S1 by amputating the parton lines associated with the diffracted proton and produced pion, and contracting them with $\gamma\cdot\hat{p}_1/2$ ($\gamma_5\gamma\cdot\hat{p}_1/2$) and $\gamma_5\gamma\cdot\hat{q}_1/2$, respectively, for the unpolarized (longitudinally polarized) GPD. The helicity amplitudes are parametrized in terms of the center-of-mass energy squared $\hat{s} = s(1+\xi)/(2\xi)$, the angles (θ,ϕ) of the pion in the SDHEP frame, and the parton momentum fractions x and z,

$$
\begin{aligned}
C_{\pm\pm}(x,z;\hat{s},\theta,\phi) &= \frac{\mathcal{N}}{\hat{s}} e^{\mp i\phi} C_+(x,z;\theta), \quad C_{\pm\mp}(x,z;\hat{s},\theta,\phi) = \frac{\mathcal{N}}{\hat{s}} e^{\mp i\phi} C_-(x,z;\theta),\\
\widetilde{C}_{\pm\pm}(x,z;\hat{s},\theta,\phi) &= \pm\frac{\mathcal{N}}{\hat{s}} e^{\mp i\phi} \widetilde{C}_+(x,z;\theta), \quad \widetilde{C}_{\pm\mp}(x,z;\hat{s},\theta,\phi) = \pm\frac{\mathcal{N}}{\hat{s}} e^{\mp i\phi} \widetilde{C}_-(x,z;\theta),
\end{aligned}
\tag{S1}
$$

where $\mathcal{N} = 2ie^2g^2C_F/N_c$ is a normalization factor, we have used parity symmetry to reduce the eight helicity amplitudes into four independent ones, the two helicity-conserving ones, C_+ and $\widetilde{C}_+$, and two helicity-flipping ones, C_- and $\widetilde{C}_-$. To present these amplitudes with the charge-conjugation symmetry manifestly exhibited, we introduce the variables $z_1 = (x+\xi)/(2\xi)$ and $z_2 = z$, such that when we picture the parton pair state $A^* = [q\bar{q}']$ as the two valence partons from a meson, z_1 and $(1-z_1)$ are the light-cone momentum fractions of the two collinear partons. This variable choice makes full advantage of the two-stage paradigm depicted in Fig. 2 [15]. Then the four independent helicity amplitudes are,

$$
\begin{aligned}
2\xi C_+(\theta;x,z) = &-(e_1-e_2)^2\left[\frac{1-\cos\theta}{1+\cos\theta}\cdot\mathcal{P}\frac{z_1+z_2-2z_1z_2}{2z_1z_2(1-z_1)(1-z_2)}\right] + (e_1^2-e_2^2)\left[\frac{2}{1-\cos\theta}\cdot\mathcal{P}\frac{z_1-z_2}{z_1z_2(1-z_1)(1-z_2)}\right]\\
&+ e_1e_2\,\mathcal{P}\left[\frac{1-\cos\theta}{z_1z_2(1-z_1)(1-z_2)}\cdot\frac{(z_1z_2+(1-z_1)(1-z_2))\,(z_1(1-z_1)+z_2(1-z_2))}{(2(1-z_1)(1-z_2)-(1+\cos\theta)z_1z_2)\,(2z_1z_2-(1+\cos\theta)(1-z_1)(1-z_2))}\right]\\
&+ i\pi\Bigg\{(e_1-e_2)^2\,\frac{2\cos\theta}{\sin^2\theta}\left(\frac{\delta(1-z_1)}{z_2}+\frac{\delta(z_1)}{1-z_2}\right) + \frac{(e_1^2-e_2^2)}{2}\cdot\frac{3-\cos\theta}{1-\cos\theta}\left(\frac{\delta(1-z_1)}{z_2}-\frac{\delta(z_1)}{1-z_2}\right)\\
&\quad - \frac{e_1e_2}{2}\left(\frac{1-\cos\theta}{1+\cos\theta}-\frac{4}{1-\cos\theta}\right)\left(\frac{\delta(1-z_1)}{z_2}+\frac{\delta(z_1)}{1-z_2}\right) - \frac{e_1e_2}{(1+\cos\theta)\,z_2\,(1-z_2)}\times\\
&\quad\times\left[\left(\frac{z_1}{1-z_2}+\frac{1+\cos\theta}{2}\frac{1-z_2}{z_1}\right)\delta\left(z_1-\rho(z_2)\right) + \left(\frac{1+\cos\theta}{2}\frac{z_1}{1-z_2}+\frac{1-z_2}{z_1}\right)\delta\left(z_1-\widetilde{\rho}(z_2)\right)\right]\Bigg\},
\end{aligned}
\tag{S2}
$$

$$2\xi C_-(\theta;x,z) = -(e_1-e_2)^2\left[\frac{1-\cos\theta}{1+\cos\theta}\cdot\mathcal{P}\frac{z_1z_2+(1-z_1)(1-z_2)}{2z_1z_2(1-z_1)(1-z_2)}\right] \tag{S3}$$
$$-i\pi\left\{\frac{(e_1-e_2)^2}{1+\cos\theta}\left(\frac{\delta(1-z_1)}{1-z_2}+\frac{\delta(z_1)}{z_2}\right)+\frac{e_1^2-e_2^2}{2}\left(\frac{\delta(z_1)}{z_2}-\frac{\delta(1-z_1)}{1-z_2}\right)+\frac{2e_1e_2}{1+\cos\theta}\left(\frac{\delta(1-z_1)}{1-z_2}+\frac{\delta(z_1)}{z_2}\right)\right\},$$

$$2\xi\widetilde{C}_+(\theta;x,z) = -(e_1-e_2)^2\left[\frac{3+\cos\theta}{2\,(1+\cos\theta)}\cdot\mathcal{P}\frac{z_1-z_2}{z_1z_2(1-z_1)(1-z_2)}\right] \tag{S4}$$
$$+e_1e_2\mathcal{P}\left[\frac{(3+\cos\theta)}{z_1z_2(1-z_1)(1-z_2)}\cdot\frac{(z_1-z_2)(1-z_1-z_2)^2}{(2(1-z_1)(1-z_2)-(1+\cos\theta)z_1z_2)\,(2z_1z_2-(1+\cos\theta)(1-z_1)(1-z_2))}\right]$$
$$+i\pi\left\{\frac{2(e_1-e_2)^2}{\sin^2\theta}\left(\frac{\delta(z_1)}{1-z_2}-\frac{\delta(1-z_1)}{z_2}\right)+\frac{e_1^2-e_2^2}{2}\frac{1+\cos\theta}{1-\cos\theta}\left(\frac{\delta(1-z_1)}{z_2}+\frac{\delta(z_1)}{1-z_2}\right)+\frac{e_1e_2}{2}\times\right.$$
$$\left.\times\left[\left(\frac{8}{\sin^2\theta}-\frac{1-\cos\theta}{1+\cos\theta}\right)\left(\frac{\delta(z_1)}{1-z_2}-\frac{\delta(1-z_1)}{z_2}\right)-\frac{1-\cos\theta}{1+\cos\theta}\frac{z_1-z_2}{z_2\,(1-z_2)}\left[\delta\left(z_1-\rho(z_2)\right)+\delta\left(z_1-\widetilde{\rho}(z_2)\right)\right]\right]\right\},$$

$$2\xi\widetilde{C}_-(\theta;x,z) = -(e_1-e_2)^2\left[\frac{1-\cos\theta}{1+\cos\theta}\cdot\mathcal{P}\frac{(1-z_1-z_2)}{2z_1z_2(1-z_1)(1-z_2)}\right] \tag{S5}$$
$$-i\pi\left\{\frac{(e_1-e_2)^2}{1+\cos\theta}\left(\frac{\delta(z_1)}{z_2}-\frac{\delta(1-z_1)}{1-z_2}\right)+\frac{e_1^2-e_2^2}{2}\left(\frac{\delta(z_1)}{z_2}+\frac{\delta(1-z_1)}{1-z_2}\right)+\frac{2\,e_1e_2}{1+\cos\theta}\left(\frac{\delta(z_1)}{z_2}-\frac{\delta(1-z_1)}{1-z_2}\right)\right\},$$

where $\mathcal{P}$ indicates that the hard coefficients should be understood in the sense of principle-value integration for z_1 (or x), when convoluted with the GPD and DA. We have expressed the amplitudes in the general flavor case with the two parton lines carrying electric charge e_1 and e_2, with $e_u = 2/3$ and $e_d = -1/3$ for u and d quarks. For charged pion $\pi^\pm$ productions, we have $(e_1, e_2) = (e_u, e_d)$ or (e_d, e_u), and all terms in Eqs. (S2)-(S5) contribute. For neutral pion production, however, we have $e_1 = e_2 = e_u$ or e_d, which cancels the terms proportional to $(e_1-e_2)^2$ and $(e_1^2-e_2^2)$.

The special gluon propagators in the type-A diagrams in Fig. S1 introduce new poles of z_1 in addition to 0 and 1,

$$\rho(z_2) = \frac{(1+\cos\theta)(1-z_2)}{1+\cos\theta+(1-\cos\theta)z_2} = \frac{1-z_2}{1+z_2\tan^2(\theta/2)}, \quad \widetilde{\rho}(z_2) = 1-\rho(1-z_2), \tag{S6}$$

both of which lie between 0 and 1 for $z_2 \in [0,1]$ and $\theta \in (0,\pi)$. They translate to poles of x at

$$x_p(\xi,z,\theta) = \xi\,(2\rho(z)-1) = \xi\cdot\left[\frac{\cos^2(\theta/2)(1-z)-z}{\cos^2(\theta/2)(1-z)+z}\right], \quad \widetilde{x}_p(\xi,z,\theta) = \xi\,(2\widetilde{\rho}(z)-1) = -x_p(\xi,1-z,\theta), \tag{S7}$$

which lie between $-\xi$ and ξ.

The convolution of the hard coefficients with the GPD H or $\widetilde{H}$ and $\bar{D}(z)$ can be simplified by using $\bar{D}(z) = \bar{D}(1-z)$. Specifically, using the notations in Eq. (2), we have

$$\mathcal{M}_+^{[\widetilde{H}]} = (e_1-e_2)^2\cdot\bar{D}_0\cdot\left[\frac{1-\cos\theta}{2(1+\cos\theta)}\cdot\widetilde{H}_0^+(\xi,t)+\frac{2i\pi\cos\theta}{\sin^2\theta}\cdot\widetilde{H}^+(\xi,\xi,t)\right]$$
$$+\left(e_1^2-e_2^2\right)\cdot\bar{D}_0\cdot\left[-\frac{2}{1-\cos\theta}\cdot\widetilde{H}_0^-(\xi,t)+\frac{i\pi}{2}\cdot\frac{3-\cos\theta}{1-\cos\theta}\cdot\widetilde{H}^-(\xi,\xi,t)\right]$$
$$+e_1e_2\cdot\left\{\int_0^1\frac{\mathrm{d}z\,\bar{D}(z)}{z(1-z)}\left[\frac{1}{2z+(1+\cos\theta)(1-z)}+\frac{2z+(1+\cos\theta)(1-z)}{2(1+\cos\theta)}\right]\cdot\int_{-1}^1\mathrm{d}x\,\frac{\widetilde{H}^+(x,\xi,t)}{x-x_p(\xi,z,\theta)+i\epsilon}\right.$$
$$\left.+\bar{D}_0\cdot\left[\frac{1-\cos\theta}{2(1+\cos\theta)}\cdot\widetilde{H}_0^+(\xi,t)-i\pi\left(\frac{1-\cos\theta}{2(1+\cos\theta)}-\frac{2}{1-\cos\theta}\right)\cdot\widetilde{H}^+(\xi,\xi,t)\right]\right\}, \tag{S8}$$

$$\mathcal{M}_-^{[\widetilde{H}]} = (e_1-e_2)^2\cdot\bar{D}_0\cdot\left[\frac{1-\cos\theta}{2(1+\cos\theta)}\cdot\widetilde{H}_0^+(\xi,t)-\frac{i\pi}{1+\cos\theta}\cdot\widetilde{H}^+(\xi,\xi,t)\right]$$
$$+\left(e_1^2-e_2^2\right)\cdot\frac{i\pi}{2}\cdot\bar{D}_0\cdot\widetilde{H}^-(\xi,\xi,t)-e_1e_2\cdot\frac{2i\pi}{1+\cos\theta}\cdot\bar{D}_0\cdot\widetilde{H}^+(\xi,\xi,t), \tag{S9}$$

$$\widetilde{\mathcal{M}}_+^{[H]} = (e_1-e_2)^2\cdot\bar{D}_0\cdot\left[\frac{3+\cos\theta}{2\,(1+\cos\theta)}\cdot H_0^+(\xi,t)-\frac{2i\pi}{\sin^2\theta}\cdot H^+(\xi,\xi,t)\right]$$
$$+\left(e_1^2-e_2^2\right)\cdot\frac{i\pi}{2}\cdot\frac{1+\cos\theta}{1-\cos\theta}\cdot\bar{D}_0\cdot H^-(\xi,\xi,t)$$

$$+ e_1 e_2 \cdot \left\{ \int_0^1 \frac{\mathrm{d}z\, \bar{D}(z)}{z(1-z)} \left[\frac{1}{2z + (1+\cos\theta)(1-z)} - \frac{2z + (1+\cos\theta)(1-z)}{2(1+\cos\theta)} \right] \cdot \int_{-1}^1 \mathrm{d}x\, \frac{H^+(x,\xi,t)}{x - x_p(\xi,z,\theta) + i\epsilon} \right.$$
$$\left. + \bar{D}_0 \cdot \left[\frac{3+\cos\theta}{2(1+\cos\theta)} \cdot H_0^+(\xi,t) - \frac{i\pi}{2} \left(\frac{8}{\sin^2\theta} - \frac{1-\cos\theta}{1+\cos\theta} \right) H^+(\xi,\xi,t) \right] \right\}, \tag{S10}$$

$$\widetilde{\mathcal{M}}_-^{[H]} = -(e_1 - e_2)^2 \cdot \bar{D}_0 \cdot \left[\frac{1-\cos\theta}{2(1+\cos\theta)} H_0^+(\xi,t) - \frac{i\pi}{1+\cos\theta} H^+(\xi,\xi,t) \right]$$
$$- \left(e_1^2 - e_2^2\right) \cdot \frac{i\pi}{2} \cdot \bar{D}_0 \cdot H^-(\xi,\xi,t) + e_1 e_2 \cdot \frac{2i\pi}{1+\cos\theta} \cdot \bar{D}_0 \cdot H^+(\xi,\xi,t), \tag{S11}$$

where we have defined the charge-conjugation-even (C-even) and charge-conjugation-odd (C-odd) GPD combinations

$$H^\pm(x,\xi,t) \equiv H(x,\xi,t) \mp H(-x,\xi,t), \quad \widetilde{H}^\pm(x,\xi,t) \equiv \widetilde{H}(x,\xi,t) \pm \widetilde{H}(-x,\xi,t), \tag{S12}$$

and the "zeroth moments" of the DA and GPDs,

$$\bar{D}_0 \equiv \int_0^1 \frac{dz\, \bar{D}(z)}{z}, \quad F_0(\xi,t) \equiv \mathcal{P} \int_{-1}^1 \frac{dx\, F(x,\xi,t)}{x-\xi}, \tag{S13}$$

for F being $H^\pm$ or $\widetilde{H}^\pm$. We note that charge conjugation symmetry on the hard coefficients are reflected as the symmetry under $(z_1, z_2) \leftrightarrow (1-z_1, 1-z_2)$ and $e_1 \leftrightarrow e_2$ [14] in Eqs. (S2)-(S5). As a result, the $(e_1 - e_2)^2$ and $e_1 e_2$ terms are probing the C-even GPD components, whereas the $\left(e_1^2 - e_2^2\right)$ terms the C-odd GPD components. Furthermore, the $(e_1 - e_2)^2$ and $\left(e_1^2 - e_2^2\right)$ terms are only related to the moments and diagonal values of GPDs, which vanish for shadow GPDs. In contrast, the $e_1 e_2$ terms contain special GPD integrals [Eq. (8)] that provide enhanced sensitivity to the x dependence of GPDs, which are capable of distinguishing shadow GPDs.

Construction of shadow GPDs

Following the spirit of Ref. [30], we define the (leading-order) shadow GPDs $S(x,\xi)$ as having null forward limits and moment integrals in Eq. (7), while having the same polynomiality and time reversal properties as normal GPDs. That is, we require

$$S(x,-\xi) = S(x,\xi), \quad S(\pm 1,\xi) = 0, \quad S(x,0) = 0, \quad S(\pm\xi,\xi) = 0, \quad \int_{-1}^1 dx \frac{S(x,\xi)}{x-\xi} = 0, \tag{S14}$$

and the $(n+1)$-th moment of $S(x,\xi)$ be an even polynomial of ξ of at most n-th order,

$$\int_{-1}^1 dx\, x^n\, S(x,\xi) = \sum_{i=0,2,\cdots}^{n} (2\xi)^i\, S_{n+1,i}\,. \tag{S15}$$

Note that we have dropped the t dependence in S, which may be introduced [31] to relax the small ξ suppression (due to $S(x,0) = 0$) in Eq. (S14), and the possible ξ^{n+1} term in Eq. (S15) which is associated with the D-term. We will construct a shadow D-term separately below. Since it is either the C-even or C-odd GPD combination [Eq. (S12)] that enters the scattering amplitude, we require $S(x,\xi)$ to be either odd or even in x, when it is to be added to H or $\widetilde{H}$. This has allowed us to leave out the condition $\int_{-1}^1 dx\, S(x,\xi)/(x+\xi) = 0$ in Eq. (S14) from which it can be inferred. Besides, we also require the first moment of the shadow GPD to vanish since that can be constrained by the electromagnetic form factor measurements, i.e.,

$$\int_{-1}^1 dx\, S(x,\xi) = S_{1,0} = 0. \tag{S16}$$

The conditions in Eq. (S14) lead to some general constraints on the shadow GPDs. In low energy scattering such as at JLab Hall-D, the accessible ξ values are small, $\xi \ll 1$. The zeros at $x = \pm\xi$ then severely constrain the shadow GPD values in the ERBL region, which can only grow up to a certain power of ξ. In this case, the integrals in Eq. (S16) and the last equation in Eq. (S14) mainly receive contributions from the DGLAP region, which must be highly suppressed. As a result, the shadow GPDs must have extra zeros in the DGLAP region, but not necessarily

in the ERBL region. Such oscillation strongly suppresses the contributions to the special integrals in Eq. (8) from shadow GPDs in the DGLAP region. This agrees with our observation in Figs. 4 and 5. In contrast, at a larger ξ, the ERBL region can become stronger, and such constraints no longer exist.

To construct specific models for shadow GPDs, we choose the following ansatz,

$$S(x,\xi) = K_0\,\xi^2\,x^a\,(x^2-\xi^2)\,(1-x^2)^b\cdot Q_{2n}(x,c), \tag{S17}$$

where $a \geq 0$, and $b, n > 0$ are integers, and $Q_{2n}(x) = 1 + c\,x^2 + \cdots + q_{2n}(c)\,x^{2n}$ is an even $2n$-th order polynomial of x. This parametrization automatically satisfies the first four conditions in Eq. (S14). Since it is only a fourth order polynomial of ξ, the polynomiality condition can be readily satisfied. We have fixed the power of $(x^2-\xi^2)$ to be unity; a higher power further suppresses the ERBL region and leads to little impact to the integrals in Eq. (8). For given a and b, we choose n to be the minimum integer such that Eq. (S17) satisfies all the conditions in Eqs. (S14)(S15) and (S16). The single parameter c is allowed to tune the shape of shadow GPD. For any given choice, we choose the normalization K_0 (independent of ξ) such that $\int_{-1}^{1} dx\,S^2(x,\xi) = 2^2$ when $\xi = 0.1$.

We choose the GK model as the standard GPDs, $H_0(x,\xi,t)$ and $\widetilde{H}_0(x,\xi,t)$, and vary them by adding shadow GPDs to the u quark GPD. For the unpolarized GPD, since the H^+ entering $I[H]$ in Eq. (8) is an odd function of x, we choose $a = 1$, $b = 2$ or 6, and $n = 3$. We choose c to make the integral $|I[S]|$ maximize, which gives $c = -11$ or -17. These two shadow GPDs, $S_1(x,\xi)$ and $S_2(x,\xi)$, make up two other models, $H_{1,2} = H_0 + S_{1,2}$. Similarly, for the polarized GPD, we choose $a = 0$, $b = 2$ or 6, $n = 3$, and $c = -24$ or -40. This gives two shadow GPDs, $\widetilde{S}_1(x,\xi)$ and $\widetilde{S}_2(x,\xi)$, and two GPD models, $\widetilde{H}_{1,2} = \widetilde{H}_0 + \widetilde{S}_{1,2}$.

For the unpolarized GPD, an additional term proportional to $\mathrm{mod}(n,2)(2\xi)^{n+1}$ can exist on the right hand side of Eq. (S15), which comes from the D-term in the double distribution representation,

$$H^q(x,\xi,t) = \int_{-1}^{1} d\beta \int_{-1+|\beta|}^{1-|\beta|} d\alpha\,\delta(x-\beta-\xi\alpha)\,f^q(\beta,\alpha,t) + \mathrm{sgn}(\xi)\,D^q(x/\xi,t)\,\theta\left(\xi^2-x^2\right)\,, \tag{S18}$$

where $D^q(x,t)$ is an odd function of x. Also, to retain the conditions in Eq. (S14), we drop the t dependence and choose the D-term $D_s(x)$ such that

$$D_s(-x) = -D_s(x), \quad D_s(1) = 0, \quad \int_{-1}^{1} dx\,\frac{D_s(x)}{x-1} = 0, \tag{S19}$$

where the subscript 's' is to remind that this D term is to be part of the shadow GPD, but not to be the requirement for the D-terms in the normal GPDs. Note that since the D-term automatically disappears in the forward limit, its magnitude does not necessarily suffer from the any suppression when ξ is small. Because of the last condition in Eq. (S19), the shadow D-term cannot be probed by the dispersion relation in the DVCS data [44, 45], but it can modify the D-term in the gravitational form factor. We choose the ansatz for the shadow D-term

$$D_s(x) = J_0\,x\,(1-x^2)\cdot\left(1 + c\,x^2 - \frac{7}{15}(3c+5)x^4\right)\,\theta(1-x^2)\,, \tag{S20}$$

with $c = 50$ and the normalization factor J_0 chosen to make $\int_{-1}^{1} dx\,D_s^2(x) = 2^2$. Adding this to the u quark GPD H_0 gives another GPD model, $H_3 = H_0 + D_s$.

These GPD models have been shown for the u quark in Fig. 3 at $t = -0.2$ GeV^2, $\xi = 0.2$, with a fixed evolution scale $\mu = 2$ GeV for the GK model. As expected, at a small ξ, the shadow GPDs are small in the ERBL region, being dominated by the DGLAP region. In Fig. S2, we show the same set of GPD models but with a larger ξ at 0.4. One can immediately notice that the shadow GPDs (not the shadow D-term) scale up with ξ very rapidly and the ERBL region becomes dominant.

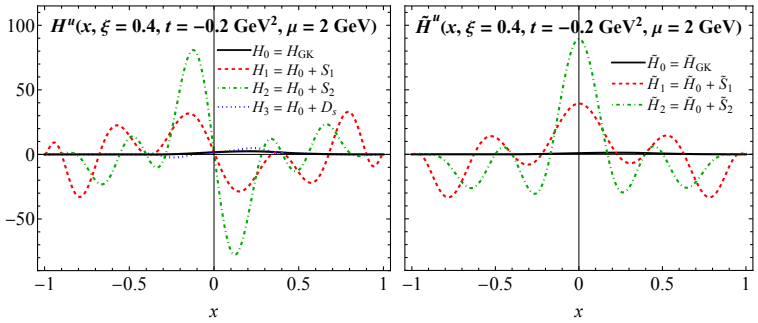

Fig. S2. Choices of the u-quark GPD models, same as Fig. 3 but at $\xi = 0.4$. The GK model (solid black line) lies very close to the horizontal axis in such a vertical scale.